International Journal of Mechanical, Industrial and Aerospace Sciences
ISSN: 2517-9950
Vol:14, No:5, 2020

Multi-Objective Optimal Design of a Cascade Control System for a Class of Underactuated Mechanical Systems

Yuekun Chen, Yousef Sardahi, Salam Hajjar, Christopher Greer

Abstract—This paper presents a multi-objective optimal design of a cascade control system for an underactuated mechanical system. Cascade control structures usually include two control algorithms (inner and outer). To design such a control system properly, the following conflicting objectives should be considered at the same time: 1) the inner closed-loop control must be faster than the outer one, 2) the inner loop should fast reject any disturbance and prevent it from propagating to the outer loop, 3) the controlled system should be insensitive to measurement noise, and 4) the controlled system should be driven by optimal energy. Such a control problem can be formulated as a multi-objective optimization problem such that the optimal trade-offs among these design goals are found. To authors best knowledge, such a problem has not been studied in multi-objective settings so far. In this work, an underactuated mechanical system consisting of a rotary servo motor and a ball and beam is used for the computer simulations, the setup parameters of the inner and outer control systems are tuned by NSGA-II (Non-dominated Sorting Genetic Algorithm), and the dominancy concept is used to find the optimal design points. The solution of this problem is not a single optimal cascade control, but rather a set of optimal cascade controllers (called Pareto set) which represent the optimal trade-offs among the selected design criteria. The function evaluation of the Pareto set is called the Pareto front. The solution set is introduced to the decision-maker who can choose any point to implement. The simulation results in terms of Pareto front and time responses to external signals show the competing nature among the design objectives. The presented study may become the basis for multi-objective optimal design of multi-loop control systems.

Keywords—Cascade control, multi-loop control systems, multi-objective optimization, optimal control.

I. Introduction

CASCADE control techniques improve significantly, in some applications, the performance of feedback controllers. Unlike single feedback control loops, cascade control strategies can act quickly to prevent external excitations from propagating through the process and making the controlled variable deviate from its desired level [1]. This important benefit has made these control methods very attractive to many applications such as chemical process industries and mechanical systems. However, the performance of the cascade control systems largely relays on the tuning of the setup parameters of both inner and outer loops [2]. Moreover, the tuning process should often satisfy multiple and often conflicting objectives. One of the main objectives in designing cascade controllers is to make the inner loop fast and responsive to minimize the effect of upsets on the primary controlled variable [1]. Other objectives such as robustness against unavoidable measurements' noise and energy-saving are also of high importance.

Yousef Hafedh Sardahi is with the Marshall University, United States (corresponding author, e-mail: sardahi@marshall.edu).

Cascade controllers have been in focus for a long time. For instance, in [2] a PID-based inner and outer control loops were designed and tuned by Maclaurin series and compared with those obtained by frequency and ITAE (integral-time-absolute error) methods. Also, in [3], a two-degree-of-freedom PID controller was designed to ensure the stability of cascade control. The outer loop gains were designed to automatically adjust their values when the inner loop controller changes. Nonlinear cascade controllers have been also found in the literature. For instance, an inner static and dynamic sliding-mode controls were designed in [4] and tested on a ball-beam system using both simplified and complete mathematical models of the system. Therein, the authors indicated that an outer loop linear controller can be implemented to further improve the stability of the system.

In this work, we discuss the design of optimal cascade controllers exploiting the concept of Multi-objective Optimization (MOP). This method allows us to optimize the design objectives simultaneously. The design problem is 4×4, four objectives and four design parameters. Details about the MOP can be found in Section II. Section III introduces the general structure of a two-level cascade control system. A numerical example of a ball-beam system is presented in Section IV. The multi-objective control problem is formulated in Section V. The optimization results are discussed in Section VI. Section VII is dedicated to concluding marks.

II. Multi-Objective Optimization

Multi-objective optimization problems (MOPs) have received much attention recently because of their enormous applications. A MOP can be stated as:

$$\min_{\mathbf{k} \in Q} \{\mathbf{F}(\mathbf{k})\}, \tag{1}$$

where $\mathbf{F}$ is the map that consists of the objective functions $f_i : Q \to R^1$ under consideration.

$$\mathbf{F} : Q \to \mathbf{R}^k, \ \mathbf{F}(\mathbf{k}) = [f_1(\mathbf{k}), \ldots, f_k(\mathbf{k})]. \tag{2}$$

$\mathbf{k} \in Q$ is a q-dimensional vector of design parameters. The domain $Q \subset \mathbf{R}^q$ can, in general, be expressed by inequality and equality constraints:

$$\begin{aligned} Q \quad = \{\mathbf{k} \in \mathbf{R}^q \mid g_i(\mathbf{k}) \leq 0, \ i = 1, \ldots, l, \\ \text{and } h_j(\mathbf{k}) = 0, \ j = 1, \ldots, m\}. \end{aligned} \tag{3}$$

where there are l inequality and m equality constraints. The solution of MOPs forms a set known as the Pareto set and the corresponding set of the objective values is called the Pareto front. The dominancy concept [5] is used to find the optimal solution. The MOPs are solved using multi-objective optimization algorithms. These methods can be classified into scalarization, Pareto, and non-scalarization non-Pareto methods [6].

The scalarization methods such as the weighted sum, goal attainment, and lexicographic approach require a transformation of the MOP into a single optimization problem (SOP [5]), normally by using coefficients, exponents, constraint limits, etc.; and then methods for single-objective optimization are utilized to search for a single solution. Computationally, these methods find a unique solution efficiently and converge quickly. However, these methods cannot discover the global Pareto solution for non-convex problems. Also, it is not always obvious for the designer to know how to choose the weighting factors for the scalarization [7].

Unlike the scalarization methods, the Pareto methods do not aggregate the elements of the objectives into a single fitness function. They keep the objectives separate all the time during the optimization process. Therefore, they can handle all conflicting design criteria independently, and compromise them simultaneously. The Pareto methods provide the decision-maker with a set of solutions such that every solution in the set expresses a different trade-off among the functions in the objective space. Then, the decision-maker can select any point from this set. Compared to the scalarization approaches, the Pareto methods can successfully find the optimal or near-optimal solution set, but they are computationally more expensive. Examples of algorithms that fall under this category are the MOGA (Multiple Objective Genetic Algorithm), PSO (Particle Swarm Optimization), NSGA-II (Non-dominated Sorting Genetic Algorithm), SPEA2 (Strength Pareto Evolutionary Algorithm), and NPGA-II (Niched Pareto Genetic Algorithm). Mainstream evolutionary algorithms for MOPs include genetic algorithm (GA), multi-objective particle swarm optimization (MOPSO), and strength Pareto evolutionary algorithm (SPEA). Deterministic methods such as set oriented methods with subdivision techniques and multi-objective algorithms based on simple cell mapping (SCM) can be also used to find the solution set [6].

The $\epsilon-$constraint and VEGA (Vector Evaluated Genetic Algorithm) approaches do not belong to either the scalarization or Pareto methods. In the $\epsilon-$constraint method, one of the cost functions is selected to be optimized and the rest of the functions in the objective space are converted into constraints by setting an upper bound to each of them. The VEGA works almost in the same way as the single objective genetic algorithm, but with a modified selection process. A comprehensive survey of the methods used for solving MOPs can be found in [8], [9], [10]. Cascade control systems can be optimally designed by using any one of these techniques.

Control systems' design problems are complex and non-convex, therefore evolutionary algorithms are methods of choice [11]. They outperform classical direct and gradient-based methods which suffer from the following problems when dealing with non-linear, non-convex, and complex problems: 1) the convergence to an optimal solution depends on the initial solution supplied by the user, and 2) most algorithms tend to get stuck at a local or sub-optimal solution. On the other side, evolutionary algorithms are computationally expensive [12]. However, this cost can be justified if a more accurate solution is desired and the optimization is conducted offline. The most widely used multi-objective optimization algorithm is the NSGA-II [13], [14]. It yields a better Pareto front as compared to SPEA2 and PESA-II (Pareto Envelope based Selection Algorithm) [15]. Therefore in this paper, we use the NSGA-II to solve the multi-objective control problem.

III. Cascade Control System

Consider the general representation of a two-level cascade control system shown in Fig. 1. The plant under control is comprised of two subsystems with transfer functions $G_1(s)$ and $G_2(s)$. An inner $C_I(s)$ and outer $C_O(s)$ control loops are used to drive the systems to their desired states. Here $X_d(s)$ and $X_o(s)$ are the desired and the actual output of the outer subsystem, respectively. While, $X_{Id}(s)$, which is computed by the outer control algorithm to attain $X_d(s)$, and $X_I(s)$ are respectively the desired and the actual output of the inner subsystem. The inner and outer load disturbances are denoted by $D_I(s)$ and $D_O(s)$, respectively. The measurement noises affecting the inner and outer feedback sensors are denoted by $N_I(s)$ and $N_O(s)$, respectively. The control system design aims to alleviate the impacts of these unwanted signals, minimize the tracking error for both control loops, make the speed of response of the inner closed-loop system faster than that of the outer one, and reduce the amount of consumed control energy. To this end, these objectives should be quantitatively described.

When deriving the design objectives, we will assume that the inner and outer closed-loop subsystems control the desired signals perfectly. This simplifies the control design and the mathematical expressions of the fitness functions that will be used later in the multi-objective optimization. Using this assumption, understanding that the design is carried out in the frequency domain, and dropping the complex variable s from the inputs and outputs, the relationship between the controlled variable, X_I and the load disturbance is denoted D_I; the tracking error of the inner closed-loop system E_2 and X_{Id}; and X_I and inner stochastic noise N_I read

$$X_I/D_I = G_1/(1 + C_I G_1), \tag{4}$$

$$E_2/X_{Id} = 1/(1 + C_I G_1), \tag{5}$$

$$X_I/N_I = (-C_I G_1)/(1 + C_I G_1), \tag{6}$$

from these equations, we notice that for better tracking, and disturbance and noise attenuation, the $\infty-$norm of the following objectives should be minimized

$$f_1 = \sup_{\omega_1<\omega<\omega_2} \sigma(\|E_2/X_{Id}\|_\infty), \tag{7}$$

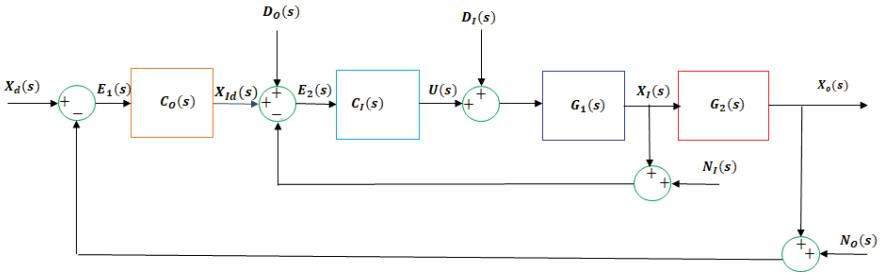

Fig. 1 Block diagram of the two-level cascade control system

$$f_2 = \sup_{\omega_3<\omega<\omega_4} \sigma(\|X_I/N_I\|_\infty). \tag{8}$$

where σ is the largest singular value among the transfer functions. The symbol sup indicates the largest gain among the gain vector elements is minimized to account for the worst-case scenario. The variables ω_1 , ω_2, ω_3, and ω_4 define the frequency ranges at which the noise and disturbance occur.

Assuming the dynamics of the inner loop which includes $C_I(s)$ and $G_I(s)$ is negligible (inner control loop is perfect), similar relationships between X_O and D_O; the tracking error of the outer closed-loop system E_1 and X_d; and X_o and inner stochastic noise N_o can be found as follows

$$X_o/D_O = G_2/(1 + C_oG_2), \tag{9}$$

$$E_1/X_d = 1/(1 + C_oG_2), \tag{10}$$

$$X_o/N_o = (-C_oG_2)/(1 + C_oG_2), \tag{11}$$

similarly, we note that for better outer loop tracking, and disturbance and noise attenuation, the norm of the following functions should be minimized

$$f_3 = \sup_{\omega_1<\omega<\omega_2} \sigma(\|E_1/X_d\|_\infty), \tag{12}$$

$$f_4 = \sup_{\omega_3<\omega<\omega_4} \sigma(\|X_o/N_o\|_\infty). \tag{13}$$

To ensure that the dynamics of the inner loop is faster than that of the outer loop, the closed-loop poles of the inner closed-loop system must be placed on the s-plane to the left of those of outer closed subsystem. This can be achieved by defining two variables λ_I and λ_o as follows:

$$\lambda_I = max(real(eig(1 + C_IG_1 = 0))), \tag{14}$$

$$\lambda_o = max(real(eig(1 + C_oG_2 = 0))), \tag{15}$$

here, eig denotes the mathematical operation that results in the eigenvalues of the corresponding equation, $real$ extracts the real part from the poles, and max returns the maximum pole. That is, these two equations return the locations of the inner and outer closed-loop dominant poles, which dictate the system speed of response. Therefore, λ_I has to be less than λ_o or the ratio λ_o/λ_I must be less than 1 to guarantee that the inner closed-loop reacts faster than the outer one.

To save the amount of control energy, we minimize the Frobenius norm, $\|.\|_F$, of the outer and inner control gains

$$f_5 = \|\mathbf{k}\|_F , \tag{16}$$

where, $\mathbf{k}$ is a vector containing the setup parameters of the control algorithms.

IV. Numerical Example

Consider the ball and beam system shown in Fig. 2. The system is comprised of two plants: the rotary servo motor and the ball and beam. The DC servo motor described by the following transfer function

$$G_1(s) = \frac{\Theta_l(s)}{U(s)} = \frac{K}{s\,(\tau s + 1)}, \tag{17}$$

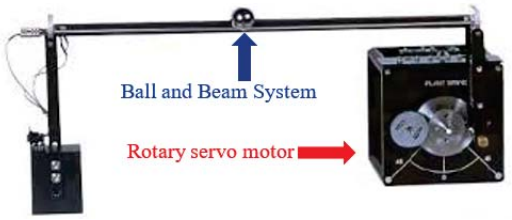

Fig. 2 Ball and beam system

where $\Theta_l(s)$ is the Laplace transform of the load shaft position $\theta(t)$, $U(s)$ is the Laplace transform of the motor input voltage $u(t)$, $K = 1.53\ rad/(V.s)$ is the steady-state gain, and $\tau = 0.0253\ s$ is the time constant. A linearized model that describes the position of the ball, $X(s)$, relative to the angle of the servo load gear reads

$$G_2(s) = \frac{X(s)}{\Theta_l(s))} = \frac{K_b}{s^2}. \tag{18}$$

Here, $K_b = 0.419\ m/(rad.s^2)$.

Now consider the general cascade control shown in Fig. 1 with $G_1(s)$ and $G_2(s)$ represent the dynamics of the DC motor and the ball-beam system, respectively. The output of the outer system, X_o, is the actual position of the ball and the output of the inner one, X_I, is the actual position of the load shaft, $\Theta_l(s)$. The desired position of the ball is denoted by X_d and the desired shaft angle is represented by X_{Id}. $N_O(s)$ is a random noise affecting the reading of the potentiometer sensor that measures the ball position, while $N_I(s)$ is the measurement noise in the DC motor angle estimation. An external excitation that alters the position of the motor's shaft

is denoted by $D_I(s)$ while that affects the position of the ball on the beam is denoted by $D_O(s)$. The inner loop implements an ideal PD (Proportional-derivative) controller to manage the position of the servo motor shaft. The controller dynamics can be described by the following transfer function

$$C_I(s) = \frac{U(s)}{E_2(s)} = K_{pi} + K_{di}s, \tag{19}$$

where, K_{pi} and K_{di} are the respectively the proportional and the derivative gains. The characteristic equation of the inner loop system, $A_I(s)$, is given by

$$A_I(s) = s^2 + \frac{1 + KK_{di}}{\tau}s + \frac{KK_{pi}}{\tau}, \tag{20}$$

the dominant pole of the inner closed-loop system can be found from

$$\lambda_I = max(real(eig(A_I(s) = 0))). \tag{21}$$

Stability analysis suggests that $K_{pi} > 0$ and $K_{di} > -1/K$ for the closed-loop system to be stable. We assume that the inner loop controller can perfectly track the desired shaft angle. With that in mind, we choose a dynamic PD controller for the outer loop

$$C_O(s) = \frac{X_{Id}(s)}{E_1(s)} = K_{do}(K_{po} + s), \tag{22}$$

here, K_{po} and K_{do} are the setup parameters of the control system. As stated above, if we assume that the inner loop can manage the dynamics of the servo motor and move the shaft to the desired position, $X_{Id}(s)$ (s), that will bring the ball to its desired location $X_d(s)$. Using this assumption, we set the closed-loop transfer function of the inner system (servo motor under PD controller) to unity. Then, the closed-loop characteristic equation of the outer loop system, $A_o(s)$, is given by

$$A_o(s) = s^2 + K_bK_{do}s + K_bK_{do}K_{po}. \tag{23}$$

as a result,the pole that dominates the dynamics of the outer control loop is given by

$$\lambda_o = max(real(eig(A_o(s) = 0))). \tag{24}$$

For the outer loop to be stable, K_{po} and K_{do} must be greater than zero. These tunable gains in addition to those of the inner controller will be tuned and the optima trade-offs among the design requirements will be found.

V. Multi-objective Optimal Design

In the multi-objective optimal design, we take the elements of the inner and outer control algorithms as the design parameters. That is $\mathbf{k}$ of (1) and (16) is given by $\mathbf{k} = [K_{pi}, K_{di}, K_{po}, K_{do}]$. The design space for the parameters is chosen as follows,

$$Q = \left\{\mathbf{k} \in [0.1, 50] \times [-0.6, 1] \times [0, 5] \times [0.1, 19] \sqsubset \mathbf{R}^4\right\}. \tag{25}$$

We notice that these ranges satisfy the stability requirements stated in (20) and (23). The MOP is stated as,

$$\min_{\mathbf{k}\in Q}\{F_1, F_2, \|\mathbf{k}\|_F, r\}, \tag{26}$$

where, $F_1 = (f_1 + f_3)/2$ is the objective that aims to enhance the tracking error and disturbance attenuation of the inner and outer closed-loop subsystems as shown in (7) and (12). The function $F_2 = (f_2 + f_4)/2$ combines the fitness functions in (8) and (13) and represents the $\infty-$norm of the transfer functions relating the output of either the inner or outer control system to the measurement noise. Measurement noises are typically dominated by high frequencies while load disturbances are dominated by low frequencies [13]. Therefore, in this paper, we assume the frequency of the noises is in the range $\omega \in [100, 10^5]\ rad/s$, while that of the disturbance belongs to $\omega \in [0.0001, 2]\ rad/s$.

Minimizing these norms ensures that the tracking error is small; the closed-loop system is insensitive to unavoidable measurements' noise and disturbances; and the control energy consumption is optimal. Furthermore, we need the response of the inner controlled system to be faster than the outer one. To this end, we minimize r given by the following equation

$$r = \lambda_o/\lambda_I. \tag{27}$$

Small values of r indicate that the inner closed-loop system is faster than the outer one, which is one of the important design requirements in cascade control loops.

To solve this multi-optimization problem, the nondominated sorting genetic algorithm (NSGA-II) is used. The reader can refer to [16] for more details about this algorithm. According to the Matlab documentation, the population size can be set in different ways and the default population size is 15 times the number of the design variables nvars. Also, the maximum number of generations should not exceed $200 \times nvars$. In this study, the population size is set to 400, and the number of generation is set to 400.

VI. Results and Discussion

Different projections of the Pareto front and Pareto set, poles' map of the inner and outer closed-loop subsystems, and the controlled system response to disturbance and measurement noise at different objective values are discussed here.

The optimization problem at hand is 4×4. That is, 4 design parameters and 4 objectives. The Pareto set which contains the optimal values of the decision variables is depicted in Fig. 3 and different projections of the corresponding Pareto fronts are plotted in Figs. 4 and 5. The color in these figures is mapped to the value of $\|\mathbf{k}\|_F$ with red denotes the highest value, and dark blue denotes the lowest value. This coloring adds a 3D projection to these figures. It also shows the corresponding design variables form the Pareto set for each point on the Pareto front. The Pareto set shows that large control energy consumption is associated with high K_{pi} and $K_{do} \times K_{po}$ values. The figure also shows that most of the optimal values of K_{po} and K_{do} are con concentrated on the right side of the graph. However, the optimal values of K_{pi} and K_{di} spread between their specified stable ranges. This can be explained

by examining (19) and (22) where the proportional gain in the latter equation is scaled by K_{do} . Empty regions indicate the non-existence of optimal solutions that satisfy the optimization constraints.

The Pareto front in Fig. 4 demonstrates a competing relationship between F_1 and $\|\mathbf{k}\|_F$, and between F_2 and $\|\mathbf{k}\|_F$. Meaning, large control energy is needed to achieve small tracking errors and better disturbance rejections (see Fig. 4 (a)). On the other side, better attenuation of the measurement noise can be only achieved when the control energy is small (see Fig. 4 (b)). That is to say, the objective of minimizing the effect of measurement noise is also conflicting with that of reducing the impact of external disturbance as shown in Fig. 5 (a)). The figure also shows that after $F_1 = 0.3$, F_2 goes up and then decrease as F_1 increases. This occurs because of the size of the objective space which includes 4 conflicting objectives. These conflicting relationships have been reported in many control books [17], [18], [19]. This stresses the fact that the design of control systems should be conducted in multi-objective settings to account for the all the trade-offs among the design targets. Another conflicting relationship between objectives can be found in Fig. 5 (b). It can be noticed that the goal of making the dynamics of the inner closed-loop system faster than that of the outer closed-loop system is in non-agreement with that of energy consumption. The pole maps of the inner and outer controlled systems are shown in Fig. 6. As indicated by the color code and the scale of the $Re(s)$-axis, the poles of the inner closed-loop system are located to the left of those of the outer controlled system. In other words, the objective to make the dynamics of the outer loop dominates that of the inner closed-loop was successfully achieved the MOP algorithm.

The responses of the inner and outer closed-loop systems at different values of r are shown in Figs. 7 and 8 when $d_i(t) = d_o(t) = 0.5sin(t)$. Here, $d_i(t)$ and $d_o(t)$ are the inverse Laplace of $D_I(s)$ and $D_O(s)$ labeled in Fig. 1. We assume that external disturbances on the inner and outer loop are low-frequency signals with period $T = 2\pi$ seconds which agrees with frequency range selected in Section V. In Fig. 7, although the response of the inner closed-loop system is almost two times that of the outer system, the tracking error is bad since the inner loop is not fast enough to prevent the propagation of the disturbance to the outer loop. While in Fig. 8, the dynamics of the inner subsystem is approximately 14 times faster than that of the outer subsystem and the result is better tracking error since the inner controlled system is fast enough to reduce the effect of the upsets on the system response. It is worth mentioning that the later response occurs at the expense of the controlled energy.

To get more insight into the ability of the system to reject unwanted signals, the time response of the controlled system $x_o(t)$, which denotes the inverse Laplace of $X_O(s)$ shown in Fig. 1, is graphed at the minimum and maximum value of the first design objective, F_1. Here, the load disturbances are modeled by the harmonic signal, $d_i(t) = d_o(t) = 0.5sin(t)$. As expected and evident from Fig. 9, the best and worst disturbance rejection occur respectively at min(F_1) and max(F_1). It should be indicated here that high control energy is required to achieve a small tracking error and better disturbance rejection. This can be readily observed from Fig. 10 where the large values of $\|\mathbf{k}\|_F$ result in better steady-state errors and repudiation of external disturbances. On the other side, small values of $\|\mathbf{k}\|_F$ are appealing for better rejection of measurement noise as shown in Fig. 11. In Fig. 11 (a), $F_2 = 0.0260$ and $\|\mathbf{k}\|_F = 8.1890$, while $F_2 = 0.3129$ and $\|\mathbf{k}\|_F = 52.5521$ in Fig. 11 (b). The outer and inner measurement noises are assumed to be white noise WN signals with 0.1 variance and zero mean; that is $n_i(t) = n_o(t) = WN$. White noise covers a wide spectrum of frequencies and is used frequently in testing controlled system behavior against sensor noises [20], [13].

VII. Conclusions

We have studied the multi-objective optimal design of a two cascaded controller based on two PD controllers. A numerical example which consists of a servo DC motor and ball-beam system is used. The optimization problem with 4 design parameters and 4 conflicting objective functions is solved with the NSGA-II algorithm. The Pareto set and front are obtained. The Pareto set includes multiple design options from which the decision-maker can choose to implement. The results show there are many optimal trade-offs among load disturbance rejection, measurement noise repudiation, control energy expenditure, tracking error reduction, and relative speed of response of the inner loop subsystem with respect to the outer one. Also, the pole maps of the control loops demonstrate that the inner closes-loop system has a faster dynamic than that of the outer controlled system. Future work will include designing optimal cascade controllers for systems that can be broken down into inner and outer dynamics; for example aeroelastic structures or aircraft wings with different numbers of ailerons.

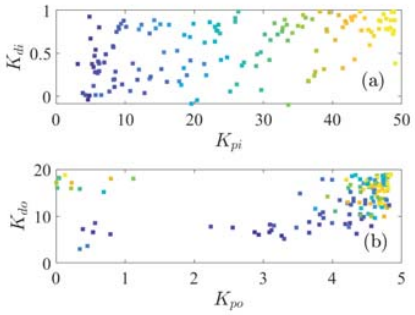

Fig. 3 Projections of the Pareto set: (a) K_{di} versus K_{pi}, (b) K_{do} versus K_{po}. The color code indicates the level of $\|\mathbf{k}\|_F$, where red denotes the highest value, and dark blue denotes the smallest

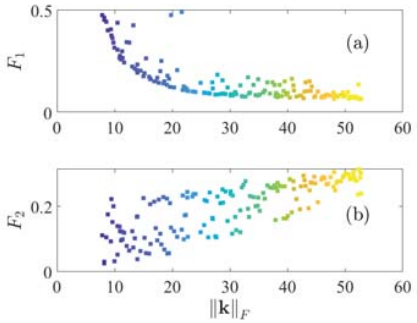

Fig. 4 Projections of the Pareto front: (a) F_1 versus $\|\mathbf{k}\|_F$, (b) F_2 versus $\|\mathbf{k}\|_F$. The color code indicates the level of $\|\mathbf{k}\|_F$, where red denotes the highest value, and dark blue denotes the smallest.

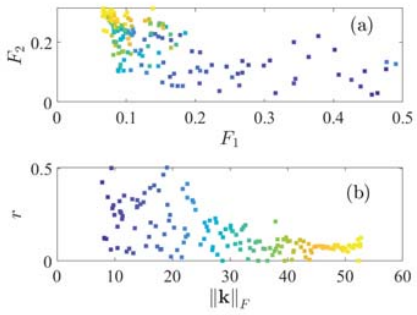

Fig. 5 Projections of the Pareto front: (a) r versus $\|\mathbf{k}\|_F$, (b) F_2 versus F_1. The color code indicates the level of $\|\mathbf{k}\|_F$, where red denotes the highest value, and dark blue denotes the smallest

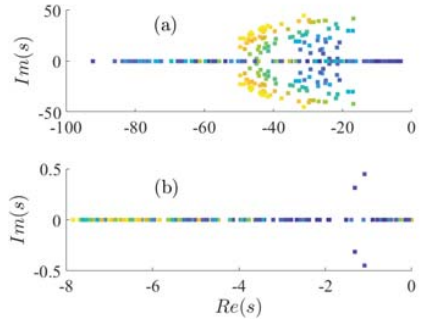

Fig. 6 Pole maps,on the y-axis is the imaginary part of the pole, $Im(s)$, and the x-axis is the real part of the pole, $Re(s)$: (a) Pole map of the inner closed-loop system, (b) Pole map of the outer closed-loop system. The color code indicates the level of $\|\mathbf{k}\|_F$, where red denotes the highest value, and dark blue denotes the smallest

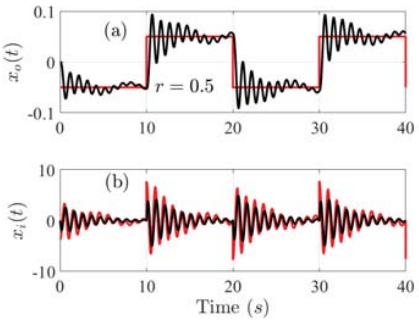

Fig. 7 Outer and inner controlled systems' responses when $r = 0.5$ (a) Response of the outer closed-loop system $x_o(t)$ versus time, (b) Response of the inner closed-loop system $x_o(t)$ versus time. Red solid line: reference signal, Black solid line: actual system, response response with $d_i(t) = d_o(t) = 0.5sin(t)$

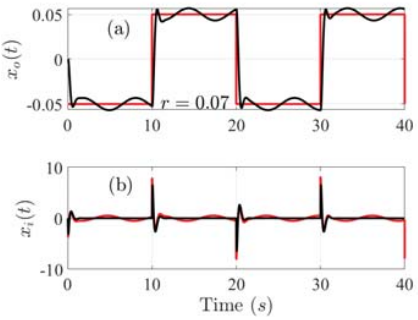

Fig. 8 Outer and inner controlled systems' responses when $r = 0.07$ (a) Response of the outer closed-loop system $x_o(t)$ versus time, (b) Response of the inner closed-loop system $x_o(t)$ versus time. Red solid line: reference signal, Black solid line: actual system, response response with $d_i(t) = d_o(t) = 0.5sin(t)$

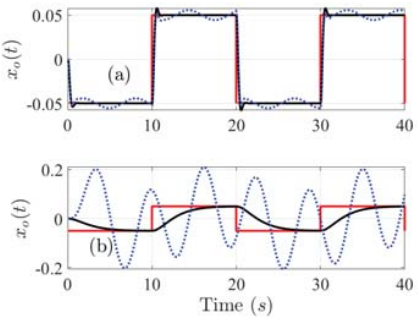

Fig. 9 Ball position versus time. (a) Controlled system response at min(F_1),(b) Controlled system response at max (F_1). Red solid line: reference signal $x_d(t)$, black solid line: system response with $d_i(t) = d_o(t) = 0$, blue dotted line: system response with $d_i(t) = d_o(t) = 0.5sin(t)$

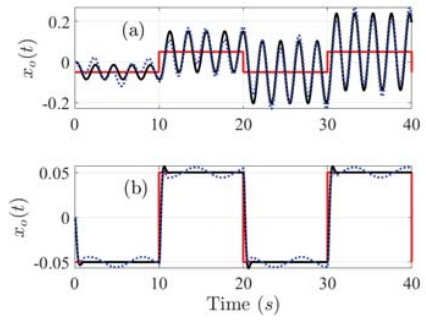

Fig. 10 Ball position versus time. (a) Controlled system response at min($\|\mathbf{k}\|_F$),(b) Controlled system response at max ($\|\mathbf{k}\|_F$). Red solid line: reference signal $x_d(t)$, black solid line: system response with $d_i(t) = d_o(t) = 0$, blue dotted line: system response with $d_i(t) = d_o(t) = 0.5sin(t)$

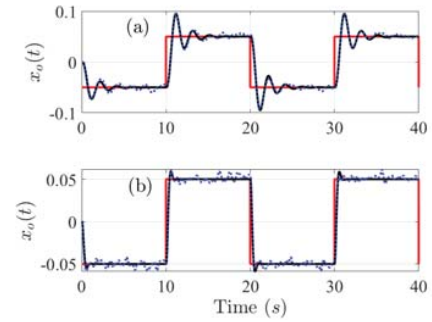

Fig. 11 Ball position versus time. (a) Controlled system response at min(F_2), (b) Controlled system response at max (F_2). Red solid line: reference signal $x_d(t)$, black solid line: system response with $n_i(t) = n_o(t) = 0$, blue dotted line: system response with $n_i(t) = n_o(t) = WN$

REFERENCES

[1] C. A. Smith and A. B. Corripio, *Principles and practice of automatic process control*. Wiley New York, 1985, vol. 2.
[2] Y. Lee, S. Park, and M. Lee, "Pid controller tuning to obtain desired closed loop responses for cascade control systems," *Industrial & engineering chemistry research*, vol. 37, no. 5, pp. 1859–1865, 1998.
[3] V. M. Alfaro, R. Vilanova, and O. Arrieta, "Two-degree-of-freedom pi/pid tuning approach for smooth control on cascade control systems," in *2008 47th IEEE Conference on Decision and Control*. IEEE, 2008, pp. 5680–5685.
[4] N. B. Almutairi and M. Zribi, "On the sliding mode control of a ball on a beam system," *Nonlinear dynamics*, vol. 59, no. 1-2, p. 221, 2010.
[5] V. Pareto *et al.*, "Manual of political economy," 1971.
[6] Y. H. Sardahi, "Multi-objective optimal design of control systems," Ph.D. dissertation, UC Merced, 2016.
[7] C. Hernández, Y. Naranjani, Y. Sardahi, W. Liang, O. Schütze, and J.-Q. Sun, "Simple cell mapping method for multi-objective optimal feedback control design," *International Journal of Dynamics and Control*, vol. 1, no. 3, pp. 231–238, 2013.
[8] D. F. Jones, S. K. Mirrazavi, and M. Tamiz, "Multi-objective meta-heuristics: An overview of the current state-of-the-art," *European journal of operational research*, vol. 137, no. 1, pp. 1–9, 2002.
[9] R. T. Marler and J. S. Arora, "Survey of multi-objective optimization methods for engineering," *Structural and multidisciplinary optimization*, vol. 26, no. 6, pp. 369–395, 2004.
[10] Y. Tian, R. Cheng, X. Zhang, and Y. Jin, "Platemo: A matlab platform for evolutionary multi-objective optimization [educational forum]," *IEEE Computational Intelligence Magazine*, vol. 12, no. 4, pp. 73–87, 2017.
[11] P. Woźniak, "Multi-objective control systems design with criteria reduction," in *Asia-Pacific Conference on Simulated Evolution and Learning*. Springer, 2010, pp. 583–587.
[12] X. Hu, Z. Huang, and Z. Wang, "Hybridization of the multi-objective evolutionary algorithms and the gradient-based algorithms," in *The 2003 Congress on Evolutionary Computation, 2003. CEC'03.*, vol. 2. IEEE, 2003, pp. 870–877.
[13] Y. Sardahi and A. Boker, "Multi-objective optimal design of four-parameter pid controls," in *ASME 2018 Dynamic Systems and Control Conference*. American Society of Mechanical Engineers, 2018, pp. V001T01A001–V001T01A001.
[14] X. Xu, Y. Sardahi, and C. Zheng, "Multi-objective optimal design of passive suspension system with inerter damper," in *ASME 2018 Dynamic Systems and Control Conference*. American Society of Mechanical Engineers, 2018, pp. V003T40A006–V003T40A006.
[15] B. Gadhvi, V. Savsani, and V. Patel, "Multi-objective optimization of vehicle passive suspension system using NSGA-II, SPEA2 and PESA-II," *Procedia Technology*, vol. 23, pp. 361–368, 2016.
[16] K. Deb, *Multi-Objective Optimization Using Evolutionary Algorithms*. New York: Wiley, 2001.
[17] R. C. Dorf and R. H. Bishop, *Modern control systems*. Pearson, 2011.
[18] K. Ogata, *Modern control engineering*. Prentice Hall Upper Saddle River, NJ, 2009.
[19] G. F. Franklin, J. D. Powell, and A. Emami-Naeini, *Feedback control of dynamic systems*. Prentice Hall Press, 2014.
[20] Y. Sardahi and J.-Q. Sun, "Many-objective optimal design of sliding mode controls," *Journal of Dynamic Systems, Measurement, and Control*, vol. 139, no. 1, p. 014501, 2017.

Yuekun Chen is a graduate student at Marshall University. Her research is focused on multi-objective optimization of cascade control systems.

Yousef Sardahi: is an assistant professor in the Mechanical Engineering Department at Marshall University. His area of expertise is control system design and optimization.

Salam Hajjar: is an assistant professor in the Electrical and Computer Engineering Department at Marshall University. Her area of expertise is embedded systems, discrete event systems, smart grids, distributed systems, and control engineering.

Christopher Greer: is a graduate student at Marshall University. His research is focused on multi-objective optimization of aeroelastic control systems.